LAWRENCE
LIVERMORE
NATIONAL
LABORATORY

UCRL-PROC-201816

Intracavity adaptive correction of a 10 kW, solid-state, heat-capacity laser.

K N LaFortune, R L Hurd, E M Johansson, C B Dane, S N Fochs, J M Brase

January 13, 2004

SPIE, Photonics West
San Jose, CA, United States
January 24, 2004 through January 29, 2004

Intracavity adaptive correction of a 10 kW, solid-state, heat-capacity laser

K. N. LaFortune[a], R. L. Hurd[a], E. M. Johansson[b], C. B. Dane[a], S. N. Fochs[a], J. M. Brase[a]

[a]Lawrence Livermore National Laboratory
[b]W. M. Keck Observatory

ABSTRACT

The Solid-State, Heat-Capacity Laser (SSHCL), under development at Lawrence Livermore National Laboratory is a large aperture (100 cm^2), confocal, unstable resonator requiring near-diffraction-limited beam quality. There are two primary sources of the aberrations in the system: residual, static aberrations from the fabrication of the optical components and predictable, time-dependent, thermally-induced index gradients within the gain medium. A deformable mirror placed within the cavity is used to correct the aberrations that are sensed externally with a Shack-Hartmann wavefront sensor. Although it is more challenging than external correction, intracavity correction enables control of the mode growth within the resonator, resulting in the ability to correct a more aberrated system longer. The overall system design, measurement techniques and correction algorithms are discussed. Experimental results from initial correction of the static aberrations and dynamic correction of the time-dependent aberrations are presented.

1. INTRODUCTION

For many applications, the optical quality of laser's output is a driving factor in its design. Often chosen for their propagation characteristics, lasers can easily perform more poorly than incoherent sources if there is no control over wavefront quality. The primary cause of wavefront degradation in many lasers is thermally-induced index gradients. Lasers can be designed to minimize the impact these thermal aberrations.[1] But, in the design of high-energy lasers, it is not always possible to design out all of the thermal aberrations. In this case, additional measures must be taken. One approach is the use of an adaptive optics control system similar to those used in astronomy.[2] Wavefront control of lasers using adaptive optics is nothing new. Typically, though, extra-cavity correction is employed because implementation is much easier than intracavity correction. However, intracavity correction provides additional benefits such as control over mode growth. Implementing an adaptive optics control system inside a resonator is difficult because there is not a one-to-one correspondence between the phase that can be measured and the phase that needs to be applied as a correction. The relationship between an intracavity corrector and the phase sensor has been well developed for an unstable resonator.[3] It can be approximated by a geometrical model. Previously, there have been experimental attempt at intracavity correction of a laser's output with adaptive optics with limited success.

2. THEORY

The system under consideration is a laser designed as a directed-energy source[4]; the objective being to deliver as many photons in as small a solid angle as possible. There are three fundamental elements to consider in the design of such systems: the size of the aperture, the optical power that can be generated, and the wavefront quality of the output. Aperture size is a concern primarily because is is inversely proportional to the divergence of the laser output. Of course, a laser of any aperture size can be expanded with a telescope before propagation to reduce its divergence angle. But, if a large aperture laser is chosen from the start, it facilitates the other considerations. For example, if a large aperture is used, it is easier to design a system that generates high optical power and yet operates far from its damage threshold or gain saturation level. The third consideration, wavefront quality, and its role in the SSHCL, will be the focus of the current discussion.

To zeroth order, the wavefront control of the system is achieved through the heat-capacity nature of the laser operation. The term "heat-capacity" refers to the fact that there is no active cooling of the laser during operation. Heat that is deposited into the system, stays there. The heat-capacity of the components, in particular

the gain medium, is used to store the heat for the duration of the laser operation. The laser must then be allowed to cool down. Although heat-capacity operation necessitates a pulsed or burst operation of the laser, it has the distinct advantage of greatly reduced aberrations over an actively cooled system. Because there is no active cooling, thermal gradients are minimized. This reduces the associated mechanical stresses. Temperature and stress dependent refractive index gradients are minimized. Deformation of the laser slabs, which also induces aberrations, is minimized. These shot-induced aberrations are still the largest component of the overall aberrations. But, they are very predictable. They depend upon the amount and distribution of heat deposited into the gain medium for each shot. This is determined by the geometry of the system and is fixed as long as the components are.

There are two other components of aberrations. The first is thermal diffusion. This is the least predictable because it depends upon the laser's history: how many shots have been fired recently and when. Fortunately, its effects cannot be seen during operation because its time constant is too long. The second is the static aberrations induced by fabrication errors in the optics. These only change when components are replaced. Thermal diffusion and static aberrations are easily compensated for either in the first few pulses of operation or immediately before operation with the probe laser because they are slowly changing. The shot-induced aberrations are more difficult to compensate for because they are larger and more rapidly changing. Fortunately, their repeatability lends them to predictive correction, which can compensate for the majority of their growth.

All of these phase errors contribute to a degradation in laser performance. Not only is the output wavefront aberrated, but the magnitude of the aberrations can be large enough to induce intensity modulation across the aperture. A problem for which extra-cavity correction does not provide a solution. Intracavity correct can provide a solution but involves a nonintuitive relationship between the output phase of the laser and the correction that must be applied to make that phase flat.

Suppose there is a phase aberration $\phi(x, z)$ within the amplifier at some longitudinal position z. That phase can be decomposed into a sum of polynomial components:

$$\phi(x, z) = \sum_n \delta_n(z) x^n. \tag{1}$$

It has been shown[5–7] that the phase at the output,

$$\phi_{out}(x, 0) = \frac{2\pi L}{\lambda} \sum_n \delta_n(z) \alpha_n(z) x^n, \tag{2}$$

can approximated by simply scaling the polynomial coefficients. The scaling coefficient $\alpha_n(z)$ represents the relative magnitude of the nth order component of the phase aberration and the phase of the laser output. It can be derived from a geometric model in the limit of small aberrations. It can be written in an analytical closed form:

$$\alpha_n(z) = \frac{1}{M^n - 1} \left(M^n + \left(1 + (M - 1) \frac{z}{L} \right)^n \right). \tag{3}$$

The coefficient L is the length of the cavity (0 is output, L is at the high-reflector), M is the geometrical magnification of the cavity and Z is the position of the aberration within the cavity. For the presented system geometry and observed aberrations, the geometrical model agrees well with the physical model and with experiment.

The control algorithm into which this geometrical scaling theory is folded comes from conventional adaptive optics. A system matrix H is found that relates the wavefront sensor's response $\vec{s}$ to any combination of actuator pushes $\vec{a}$. In practice, this is found experimentally by pushing each actuator one at at time.

$$\vec{s} = H\vec{a} \tag{4}$$

The system is designed such that the matrix H is overdeterimed. The matrix H can then be inverted using a singular-value decomposition. The resulting control matrix, $H^\dagger$, is the pseudoinverse if H and gives the best fit (in a least-squared sense) of actuator pushes given an arbitrary wavefront sensor signal:

$$\vec{a} = H^\dagger \vec{s} \tag{5}$$

Some modifications are necessary to incorporate the scaling coefficients that appear in an intracavity adaptive optics system. Since, the wavefront sensor slope measurements are not directly related to the phase of the desired correction on the DM, the scaling law described above must be used to modify the wavefront sensor response to something that is directly related to the phase of the desired correction. Equation 4 can be broken down into

$$\vec{s} = FD\vec{a} \tag{6}$$

where F is known as the finite difference matrix. It is a discrete derivative operator that transforms the phase into slopes. The D matrix relates the position, or phase, of the DM surface to actuator voltages.

The wavefront phase can be obtained from the wavefront sensor slopes by integrating them over the aperture:

$$\vec{\phi} = F^{-1}\vec{s}. \tag{7}$$

A least-squares polynomial fit to the reconstructed phase can be obtained in a matrix representation. The polynomial coefficients are

$$\vec{c} = P\vec{\phi} \tag{8}$$

where P is a matrix representation of all the polynomial coefficients that are to be fit. The polynomial fit can then rescaled using Oughstun's gain coefficients $\alpha_n(z)$, described above. A matrix W is created by putting the gain coefficients for each polynomial term along the diagonal. The new polynomial coefficents

$$\hat{c} = W\vec{c} \tag{9}$$

can then be used to reconstruct a rescaled phase

$$\hat{\phi} = P\hat{c}. \tag{10}$$

Differentiating the rescaled phase, effective wavefront sensor slopes can be calculated

$$\hat{s} = F\hat{\phi} \tag{11}$$

to which the actuator responses are now linear.

$$\hat{a} = H^{\dagger}\hat{s} \tag{12}$$

If all matrix multiplications are written together,

$$\hat{a} = H^{\dagger}FP^{-1}WPF^{-1}\vec{s}, \tag{13}$$

it can be easily seen that in the limit of unity gain (W becomes the identity matrix), this reduces to Equation 5. All of these matrix multiplications can be calculated off-line and do not add any computational overhead to the adaptive optics control loop.

3. SYSTEM DESIGN

The intracavity, adaptive-optic resonator (Figure 1), is built into the second-generation, solid-state, heat-capacity laser at LLNL. This laser is capable of producing 10 kW of average power @ 1053 nm. It is a pulsed laser, running at up to 20 Hz for a burst of up to 200 shots. After each burst, the laser is allowed to cool. Each pulse is 500 μsec long. The clear aperture is a square 10 cm on a side. The geometry of the resonator is confocal and unstable with a magnification of 1.5. The output profile of a laser with such a geometry is a square annulus with inner dimensions of 6 2/3 cm on a side.

The wavefront must be measured and controlled within the whole 10 cm by 10 cm area. Therefore a beam splitter is used within the cavity to couple out the full beam profile to the diagnostics. In addition to far-field and near-field diagnostics, there is a Shack-Hartmann wavefront sensor (WFS), which is used to measure the gradient of the phase. The WFS is made using a rectangular array of lenslets mounted in front of a camera.

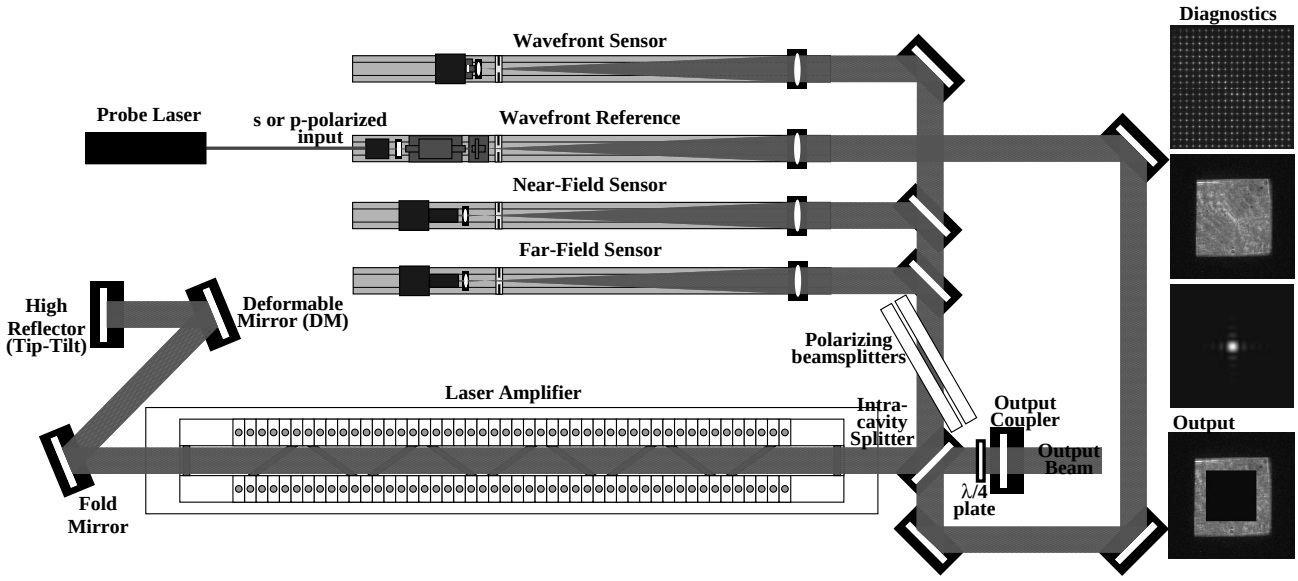

Figure 1. The system layout of the adaptively-corrected, unstable resonator. Shown are the three diagnostic paths and representative images of their output: Shack-Hartmann wavefront sensor, near-field and far-field cameras. Polarization selection is used to probe the cavity. The deformable mirror and tip-tilt correction are both at one end of the cavity. The amplifier contains nine flashlamp-pumped Nd:glass slabs at Brewster's angle. The output of the laser is a square annulus.

The gradient of the phase is sampled on a 19 by 19 grid. The average phase within each sampling interval is measured. The sensor was designed for a sensitivity of $< \lambda/10$.

The deformable mirror (DM) is designed to work with the WFS to compensate for the measured aberrations. Manufactured by Xinetics Corp., it has a ULE face-sheet, supported by 206 PMN actuators on a pseudo-hexagonal grid with a nominal 1 cm actuator spacing It was designed with a dynamic range of 10 μm, larger than the maximum observed aberration occurring in the system during its designed run time . There are 126 actuators within the clear aperture of the laser. It was manufactured to a tolerance of $< \lambda/50$ RMS powered figure. It has a high-damage-threshold, high-reflectivity, multilayer-dielectric coating.

The WFS is calibrated with a probe laser. First, the probe laser is sent directly to the WFS bypassing the cavity, to determine a reference point. Then the probe laser is propagated through the cavity. Each actuator on the DM that is within the clear aperture is pushed, one at a time. The WFS response to each impulse is recorded to generate the system matrix H from Equation 4. From all of the impulse response measurements, a matrix can be built that applies a least-squares fit of the DM surface to any measured wavefront error. The general method of operation of the control system is shown in Figure 2. The details of the control system are discussed in the following section.

4. EXPERIMENTAL RESULTS

The commissioning of the laser was done in three stages. First, was the precorrection of the static aberrations in the system due to the sum of the fabrication irregularities in all of the optical components. This was done to confirm that, in practice, it was possible to reduce the wavefront distortion in a laser using a CM to compensate for distributed aberrations at a single plane. This was done using the probe laser, passing through the cavity for one round-trip, and a conventional adaptive optics control algorithm. Figure 3 illustrates the progress along this first stage. The progress in this stage culminates in a repeatable performance level having a Strehl ratio of about 0.20 and as high as 0.26. This level of performance was sufficient for work to begin on the next step.

Second, it was important to insure that the wavefront distortion could be accurately measured. In Figure 4, nontrivial wavefront slope information has been combined with the near-field amplitude to reconstruct the far-field diffraction pattern, This pattern, when compared to the measured far-field patter, shows striking similarity.

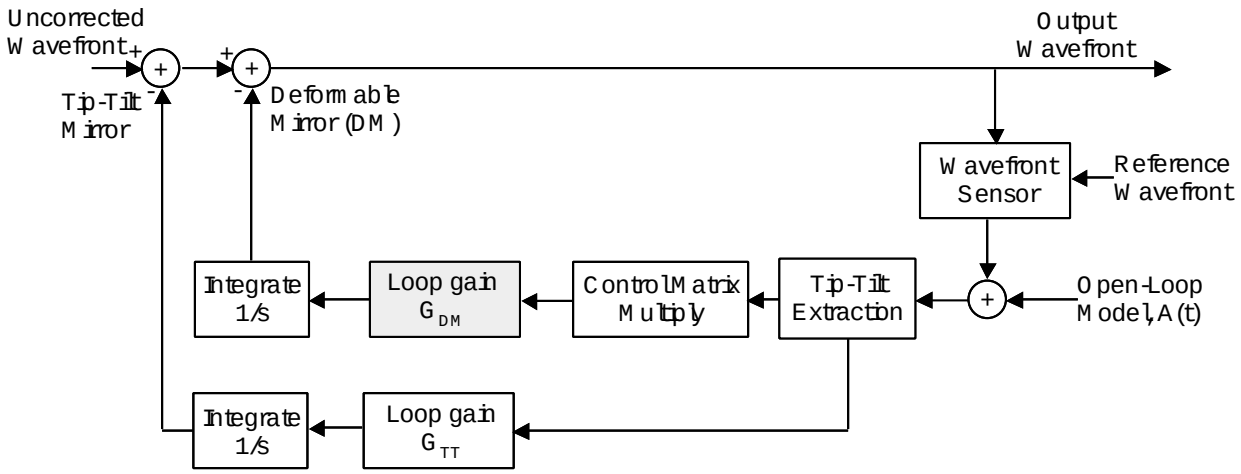

Figure 2. Flow diagram of the adaptive optics control system. A fraction of the laser output is coupled into a Shack-Hartmann wavefront sensor. The tip-tilt component of the resulting wavefront measurement is offloaded to a separate control loop. The higher-order aberrations are corrected with the deformable mirror. Predictable aberrations can be anticipated by incorporating their expected contribution into the wavefront sensor measurement.

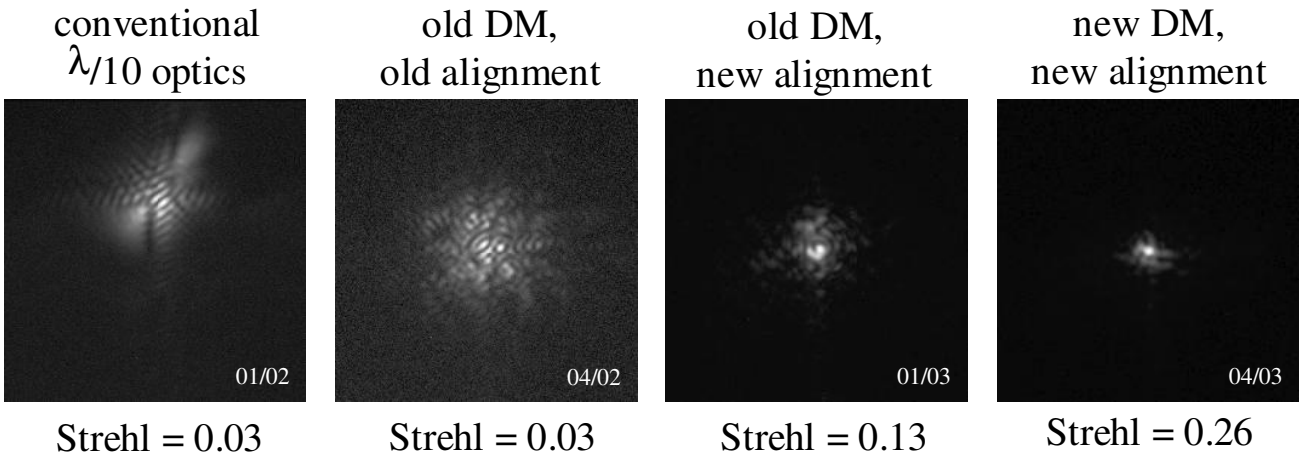

Figure 3. Initial efforts to correct the wavefront of the laser with an intracavity deformable mirror were made using measurements taken with a probe laser. The objective is to apply the proper contour to the DM such that the wavefront repeats itself after one round-trip through the cavity. Reference and test paths were set up that differ by one round-trip through the cavity. Conventional adaptive optics techniques and a null-seeking algorithm could be used. Logarithmic plots of the intensity distribution in the far-field diagnostic at various stages of development are shown with a theoretical distribution for reference.

By taking advantage of this redundancy in the diagnostics, it could be concluded that the WFS returned an accurate representation of the phase of the high-poser laser.

Third, it had to be determined that the appropriate correction could be applied to the DM. This was not obvious, given the nonlinearity of the relationship between the WFS and the DM. The phase information retrieved from the WFS was no longer based on a probe laser sent for one round trip through the cavity. It was based on the high-power laser output. Also of concern was the magnitude of the error that needed to be predictively compensated. Figure 5 illustrates multiple shots within a multi-shot run. While the shape changes from shot to shot, its overall size does not increase. The spot becomes elongated in the horizontal direction because this is the direction of the largest cumulative aberrations.

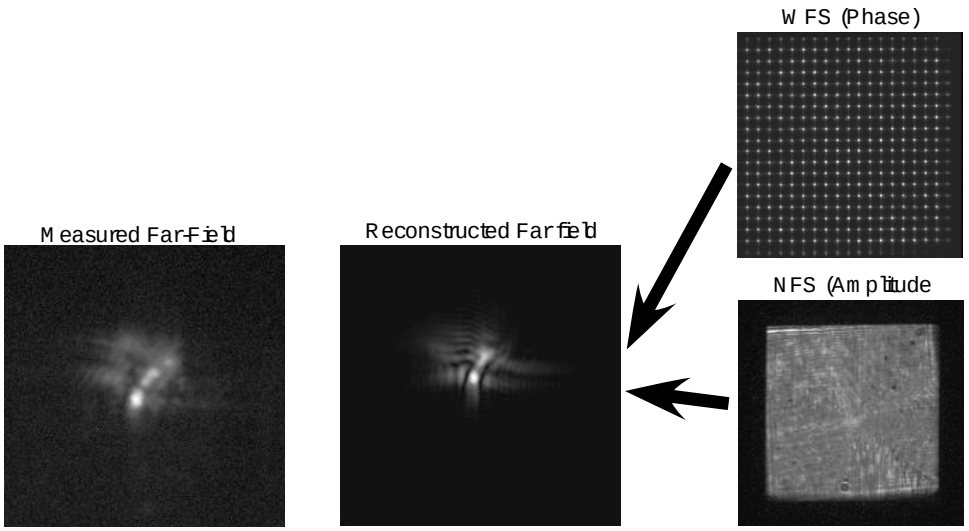

Figure 4. The redundancy in the diagnostics made it possible to confirm their accuracy. Measured far-field images were compared to those calculated using the phase information from the wavefront sensor and the amplitude information from the near-field sensor. A nontrivial example is shown.

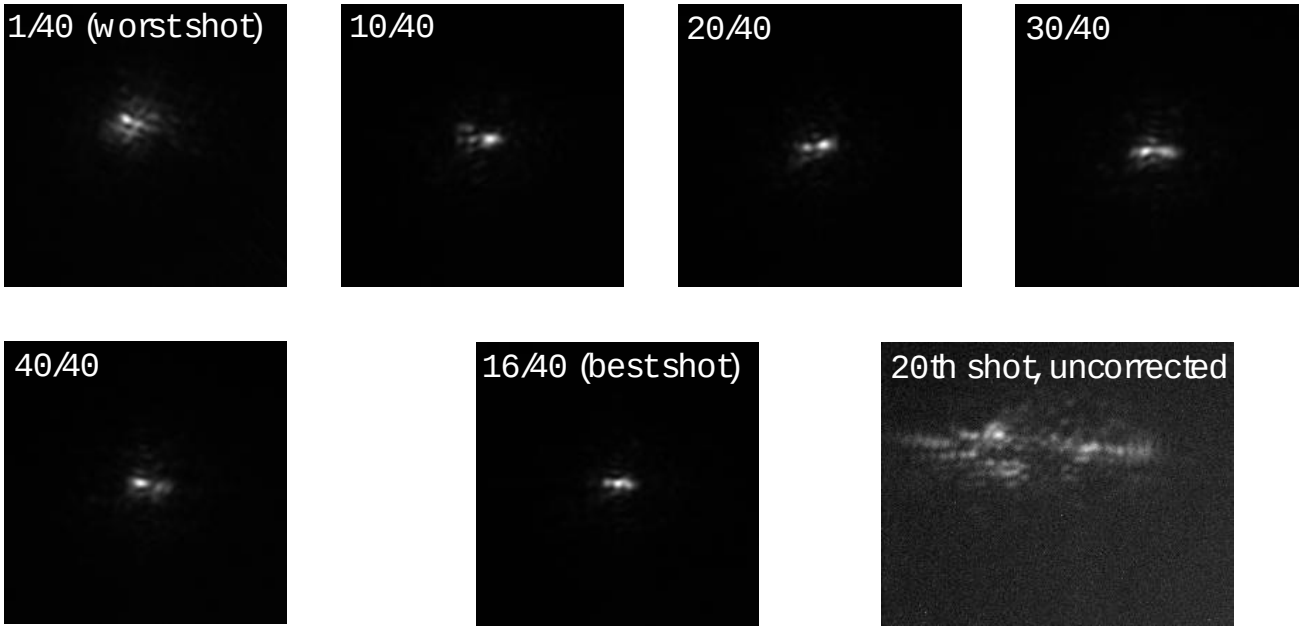

Figure 5. Far-field images of selected pulses showing the laser performance during a 40 pulse run. The best pulse (as measured by a power-in-a-bucket analysis) is shown. For comparison, the 20th pulse from a run during which no compensation for thermal aberrations took place.

The metric for performance is somewhat a matter of preference. There are many metrics to choose from, some more appropriate than others depending on the nature of the beam to be characterized. Residual wavefront error is an option but not a very good one because it does not tell you anything about the energy distribution at the target. It is more appropriate to quantify the energy distribution of the diffraction pattern rather than the phase distribution in the near-field. If the propagating beam is Gaussian, M^2 may me the appropriate choice. A Strehl ratio is useful if the operating regime is one in which the feature size or the propagation distance is

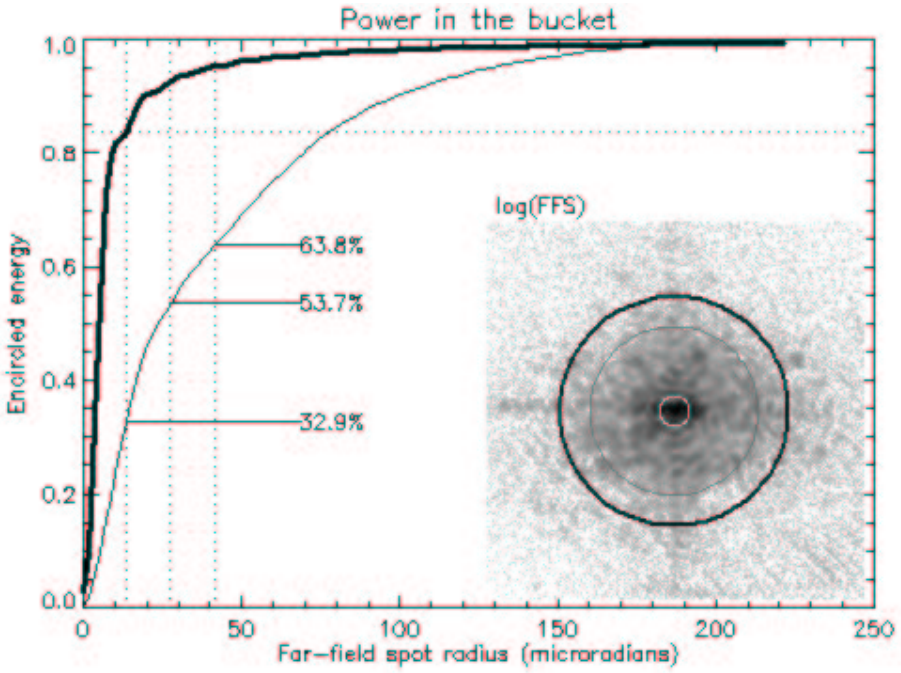

Figure 6. Power-in-a-bucket plot of the best (16 th) pulse from the sequence in Figure 5. The diffraction limited spot size is the radius to the first minimum. Vertical dotted lines are drawn at the 1x, 2x and 3x diffraction-limited radii. The fraction of the total energy contained within each of these radii is shown. A logarithmic plot of the far-field diffraction pattern ins shown. Superimposed are circles depicting the diffraction limited area (smallest), the times-diffraction limited (xDL) area (middle) and the spatial frequency domain of the DM (largest). The horizontal scale is the divergence angle assuming 1 μm light propagating from a 10 cm aperture.

large enough that only the central lobe of the far-field diffraction pattern will be used. The ratio of the actual spot radius to the theoretical limit, or "times-diffraction-limit" (xDL) number is more generally useful but is somewhat arbitrary. Different conventions are used to determine the radius. Although the temptation to reduce the wavefront quality to one number is great, a more descriptive metric is the encircled-energy, or power-in-a-bucket (PIB), curve. It is a plot of the fraction of energy contained within a radius as a function of the radius. It is, by definition, zero at a radius of zero and one at a radius of infinity. In between, one can find the xDL size (using any desired convention). The fraction of energy deposited within any desired divergence angle can be obtained. The Strehl ratio can also be estimated from the figure as the fraction of the energy within a 1xDL radius. A power-in-a-bucket curve for one of the pulses in the 40 shot run presented above appears in Figure 6. Line-outs of the same pulse appear in Figure 7. To perform a reliable PIB measurement, a 12 bit camera with low read noise (< 2 counts) and a large area (six times the area shown) needed to be used. Careless background subtraction or lower bit-depth resulted in artificially low xDL values.

5. CONCLUSION

Adaptive control of the unstable resonator in the solid-state, heat-capacity laser using a deformable mirror was achieved. Precorrection for static aberrations using a probe laser provided an initial beam quality with a Strehl of > 0.2. Measurements of the phase of the high-energy laser were made using a Shack-Hartmann wavefront sensor. The accuracy of these measurements was confirmed using redundancy in the diagnostics. A control algorithm was applied in response to the active measurements that maintained a Strehl of > 0.1. Encircled energy analyses showed that, in some pulses, nearly 33% of the laser energy fell within the diffraction limited divergence angle. Reliably, $> 60\%$ of the energy fell within three times the diffraction limited divergence angle.

Performance will continue to be optimized. Work has also begun on a next-generation system that is capable of working at a higher average power and higher repetition rate.

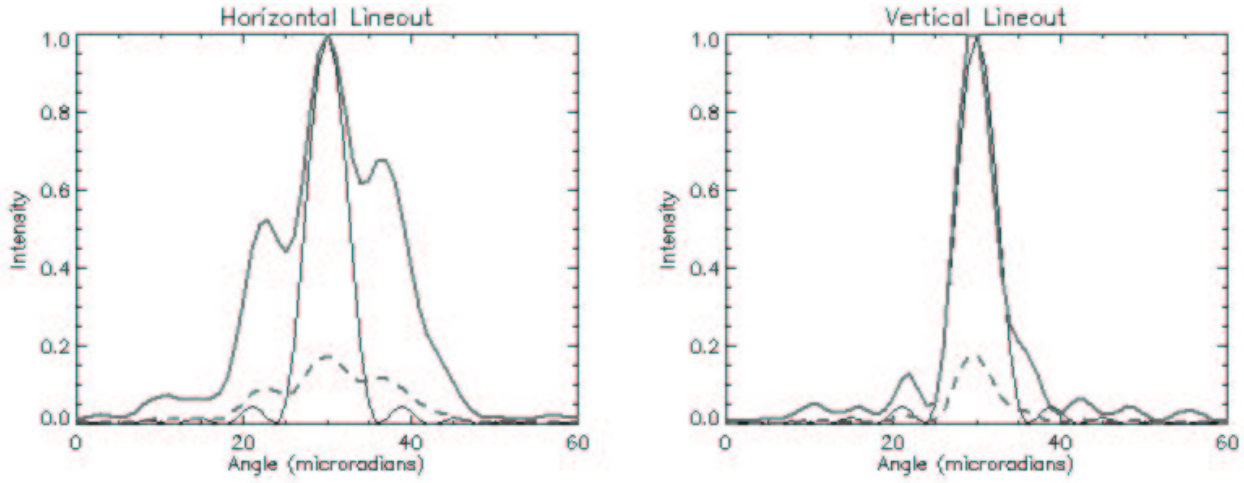

Figure 7. Horizontal and vertical line-outs of the best (16 th) pulse from the sequence in Figure 5. The peak-normalized intensity curve (thick, solid) and energy-normalized curve (thick-dashed) are compared to the theoretical limit (thin, solid). The energy-normalized curve reveals the Strehl ratio. The horizontal scale is the divergence angle assuming 1 μm light propagating from a 10 cm aperture.

Acknowledgements

Supported by U.S. Army Space and Missile Defense Command. This work was performed under the auspices of the U.S. Department of Energy by University of California, Lawrence Livermore National Laboratory under Contract W-7405-Eng-48.

REFERENCES

1. V. J, "Solid-state high-energy laser," *Proc. SPIE* **4632**, pp. 104–14, 2002.
2. C. E. Max, D. T. Gavel, and S. S. Olivier, "Near infra-red astronomy with adaptive optics and laser guide stars at the keck observatory," *Proc. SPIE* **2534**, pp. 412–22, 1995.
3. K. E. Oughstun, "Aberration sensitivity of unstable-cavity geometries," *J. Opt. Soc. Am. A - Optics & Image Science* **3**, pp. 1113–41, Aug. 1986.
4. J. Hecht, "Solid-state high-energy laser weapons," *Optics & Photonics News* **14**, pp. 42–7, Jan. 2003.
5. K. E. Oughstun, "Intracavity adaptive optic compensation of phase aberrations. i. analysis," *J. Opt. Soc. Am.* **71**, pp. 862–72, Jul. 1981.
6. K. E. Oughstun, "Intracavity adaptive optic compensation of phase aberrations. ii. passive and active cavity study for a large n_{eq} resonator," *J. Opt. Soc. Am.* **71**, pp. 1180–92, Oct. 1981.
7. K. E. Oughstun, "Theory of intracavity adaptive optic mode control," *Proc. SPIE* **365**, pp. 54–65, 1983.